Nanoscale Advances

PAPER

View Article Online
View Journal | View Issue

Check for updates

Cite this: *Nanoscale Adv.*, 2021, **3**, 6223

Selective suppression of {112} anatase facets by fluorination for enhanced TiO_2 particle size and phase stability at elevated temperatures†

Emerson C. Kohlrausch,[ab] Roberto dos Reis, [c] Rhys W. Lodge, [b] Isabel Vicente,[d] Alexandre G. Brolo, [e] Jairton Dupont, [a] Jesum Alves Fernandes [*b] and Marcos. J. L. Santos [*a]

Received 30th June 2021
Accepted 26th August 2021

DOI: 10.1039/d1na00528f

rsc.li/nanoscale-advances

Generally, anatase is the most desirable TiO_2 polymorphic phase for photovoltaic and photocatalytic applications due to its higher photoconductivity and lower recombination rates compared to the rutile phase. However, in applications where temperatures above 500 °C are required, growing pure anatase phase nanoparticles is still a challenge, as above this temperature TiO_2 crystallite sizes are larger than 35 nm which thermodynamically favors the growth of rutile crystallites. In this work, we show strong evidence, for the first time, that achieving a specific fraction (50%) of the {112} facets on the TiO_2 surface is the key limiting step for anatase-to-rutile phase transition, rather than the crystallite size. By using a fluorinated ionic liquid (IL) we have obtained pure anatase phase crystallites at temperatures up to 800 °C, even after the crystallites have grown beyond their thermodynamic size limit of *ca.* 35 nm. While fluorination by the IL did not affect {001} growth, it stabilized the pure anatase TiO_2 by suppressing the formation of {112} facets on anatase particles. By suppressing the {112} facets, using specific concentrations of fluorinated ionic liquid in the TiO_2 synthesis, we controlled the anatase-to-rutile phase transition over a wide range of temperatures. This information shall help synthetic researchers to determine the appropriate material conditions for specific applications.

Introduction

Surface chemistry plays a crucial role in the properties of solid-state materials, especially in nanoparticles where high surface-area-to-volume ratios amplify the unique physicochemical characteristics of highly energetic surface atoms.[1] Significant efforts have been devoted to controlling nanoparticle facets to produce materials with predictable optical, electrical, and catalytic properties.[2–4] The surface energy of these facets contributes to the minimization of the total surface energy of the particle during crystal growth, which can be controlled, to a certain degree, by certain synthetic approaches.[5–7]

One of the most explored approaches to control the size, shape, and catalytic properties of TiO_2 is through the incorporation of dopants, such as transition metals (Fe, Ni, Co) or non-metals (N, F, S).[8–16] The effect of fluorine on the size, phase, and morphology of TiO_2 particles has been widely explored and hydrofluoric acid has been found to be the key reactant to obtain nanoparticles with their surface dominated by exposed {001} facets.[17] Urea and EDTA have also been found to drive the formation of TiO_2 nanoparticles with large {001} facets.[18–20] Adjusting the fluoride/titanium molar ratio controlled the size of TiO_2 sheets with predominant {001} facets which was shown to improve the photodegradation efficiency of organic dyes.[21] {001} facets on uniform anatase TiO_2 single crystals were also selectively grown using hydrofluoric acid as a morphology controlling agent.[22] More recently, another study of TiO_2 growth using HF showed that whilst fluorine was responsible for the anatase morphology with exposed low-index facets, H^+ was responsible for increasing the percentage of {001} facets.[23] When TiO_2 was synthesized in fluorinated ionic liquids, it preferentially formed the brookite phase, rather than anatase, above a certain concentration of $[BF_4]^-$ anions. Subsequent thermal treatment led to a transition from brookite to anatase that was accompanied by the release of fluorine, through which the authors concluded that fluorine was responsible for stabilizing the brookite phase.[24]

[a]*Instituto de Química – UFRGS, 91501-970, Porto Alegre, RS, Brazil. E-mail: mjls@ufrgs.br*
[b]*School of Chemistry, University of Nottingham, University Park, Nottingham, NG7 2RD, UK. E-mail: jesum.alvesfernandes@nottingham.ac.ik*
[c]*Department of Materials Science and Engineering, Northwestern University, Evanston, Illinois 60208, USA*
[d]*Unitat de Tecnologíe Químiques, EURECAT, Tarragona, 43007 Spain*
[e]*Department of Chemistry, University of Victoria, P. O. Box 3065, V8W 3V6, BC, Canada*

† Electronic supplementary information (ESI) available: Experimental section, Fig. S1–S12 and Tables S1–S11, which provide more details and comprehensive image analysis. See DOI: 10.1039/d1na00528f

Of the notable facets of anatase, the {112} facet is important because it plays a crucial role in the anatase-to-rutile phase transitions. Penn *et al.* have demonstrated that rutile nucleate at {112} twin anatase interfaces.[25] Recently, Zhu *et al.*[26] have studied the pathways of surface restructuring, showing that {112} undergoes reconstruction that can lead to a new phase propagating into the anatase bulk, while the reconstruction of (001), (100), (101), and other planes only takes place at the surface. Therefore, they concluded that only the {112} in anatase is responsible for the initial nucleation that will allow anatase-to-rutile phase transition.

Furthermore, the TiO_2 crystallite size is dependent on the thermodynamic stability of each polymorphic phase. For crystallites smaller than 35 nm, the anatase phase is more stable than rutile, and an anatase-to-rutile phase transition only starts after the thermodynamic critical size is reached (>35 nm) which usually occurs at temperatures above 500 °C.[27–30] However, the growth of pure anatase phase TiO_2 nanoparticles larger than 35 nm at temperatures above 500 °C has yet to be reported as they are thermodynamically unfavorable.[31–33]

In this work, we attempted to synthesize pure anatase phase TiO_2 nanoparticles larger than 35 nm in a fluorinated ionic liquid, 1-butyl-3-methylimidazolium tetrafluoroborate ($BMIm \cdot BF_4$), at temperatures up to 800 °C and compare their efficiency with that of pure TiO_2 nanoparticles when applied to dye-sensitized solar cells (DSSCs). By using XRD diffraction patterns from thermally treated nanoparticles in a wide range of temperature, we have used the Wulff construction to extract meaningful information about facet growth on the TiO_2 particles.[34–36]

Experimental section

Synthesis of TiO_2

TiO_2 nanoparticles were synthesized by adding acetic acid (5.7 mL) to titanium isopropoxide (15 mL) under constant stirring at 25 °C.[37] The solution was stirred for 15 min and poured into deionized water (70 mL). The mixture was stirred for one hour at room temperature to complete the hydrolysis. The ionic liquid (IL) $BMIm \cdot BF_4$ (1% or 10% w/w, with respect to deionized water) was then added to the solution, in addition to nitric acid (63%, 1 mL), before being stirred for 8 hours at 80 °C. Finally, the mixture was transferred to an autoclave and heated at 230 °C for 12 hours. All samples were subsequently rinsed with water (3 × 50 mL) followed by ethanol (3 × 50 mL). The samples were labelled as TiO_2 (no addition of IL), TiO_2/IL 1% (1% (w/w) of the ionic liquid) and TiO_2/IL 10% (10% (w/w) of the ionic liquid). The samples were thermally treated at 300, 400, 500, 600, 700, 800 and 900 °C for 3 hours in air.

Characterization

The morphology, size and structural characteristics of the as-synthesized TiO_2 nanoparticles were observed by transmission electron microscopy performed with a Libra Zeiss 120 and a Philips CM300. SEM images were obtained using a JEOL 7100F Field-Emission Gun Scanning Electron Microscope (FEG-SEM). A working distance of 10 mm was maintained with acquisitions utilizing a beam voltage of 15 kV. For analysis, a small amount of the sample was deposited onto double-sided carbon tape mounted on a stub, followed by sputter-coating with iridium (5 nm thickness) to make the sample conductive. X-ray powder diffraction (XRD) patterns were obtained using a Siemens D5000 diffractometer with Cu-Kα radiation (λ = 1.5418 Å) in a 2θ range from 10 to 90° with a step size of 0.05° and time of 1 s per step.

Wulff grain construction

The Wulff grain construction was obtained by inputting the Miller indices and respective crystallite size for the {*hkl*} plane families {101}, {103}, {004} and {112} from the anatase phase with the auxiliary of VESTA software. The size of each family's planes was obtained using the Scherrer equation from XRD patterns obtained in the present work. Wulff construction was performed using the atomic position set and the space group of the anatase structure $I4_1/amd$, no. 141. The unit cell is defined by the lattice vectors *a* and *c* and contains two TiO_2 units with Ti ions at 4b Wyckoff positions (0, 1/4, 3/8) and (0, 3/4, 5/8) and O ions at 8e Wyckoff positions (0, 1/4, *u*), (0, 3/4, 1/4 + *u*), (1/2, 1/4, $-u$ + 1/2) and (1/2, 3/4, 1/4 − *u*).[38,39]

DSSC assembly and measurements

The procedure used to assemble the DSSCs followed a previous literature method.[37] The characterization and performance of the DSSCs were evaluated by current *versus* potential measurements, and carried out using a 300 W xenon arc lamp and an AM1.5 filter. The power of the simulated light was calibrated to 100 mW cm^{-2} and recorded by a picoamperimeter (Keithley, model 2400).

Results and discussion

HR-TEM investigations of TiO_2, TiO_2/IL 1% and TiO_2/IL 10% were carried out after different synthetic steps. TEM images were acquired for all samples after the hydrolysis step and, while no formation of anatase seeds was observed from TiO_2, Fig. 1 shows the formation of anatase nanoseeds from TiO_2/IL 1% and TiO_2/IL 10% (Fig. 1a, b and d, e, respectively).[40–43] After the autoclave step at 230 °C, crystalline particles were obtained for all the samples, and no significant variation in morphology, crystalline structure, or size distribution was observed (Fig. S1 and S2†).

To track TiO_2 phase transitions, and to evaluate the thermal stability of the anatase crystals, the samples were thermally treated at 300, 400, 500, 600, 700, 800 and 900 °C (Fig. 2 and S3†). For TiO_2, the phase transition of anatase-to-rutile began at 400 °C with a small diffraction peak at *ca.* 27.4°. As the temperature rose to 600 °C, a sharper, defined diffraction peak at *ca.* 27.4° was observed (Fig. 2a). The calculated TiO_2 crystallite sizes at 600 °C were 24.4 and 36.2 nm for anatase and rutile, respectively (Fig. 3b and Table S1†). A complete conversion to rutile took place between 700 and 800 °C resulting in rutile crystallites 43.0 nm in size. At 700 °C, only a small number of

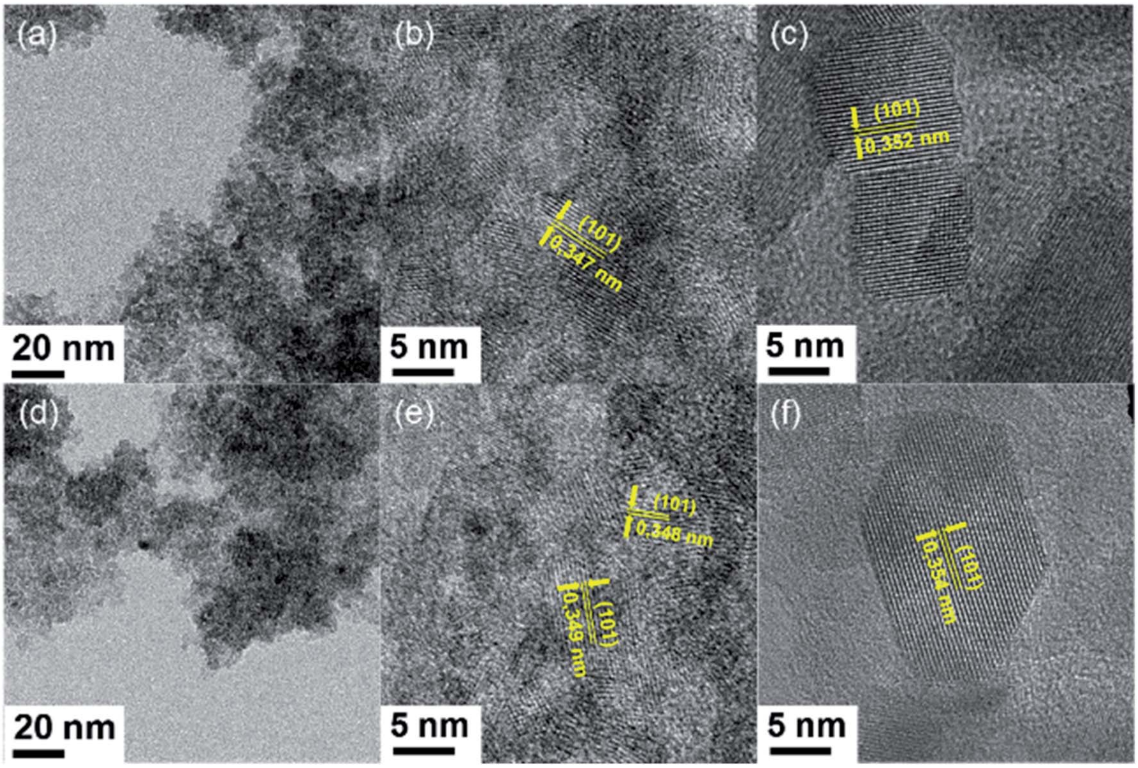

Fig. 1 TEM images obtained after hydrolysis at 80 °C from TiO_2/IL 1% (a and b) and TiO_2/IL 10% (d and e). HRTEM images obtained after hydrothermal reaction at 230 °C from TiO_2/IL 1% (c) and TiO_2/IL 10% (f).

anatase particles with a crystallite size of 28.2 nm were observed. For TiO_2/IL 1% (Fig. 2b), the anatase-to-rutile phase transition started at *ca.* 800 °C with anatase presenting a crystallite size of 42.8 nm and an incomplete conversion of anatase-to-rutile being observed even at 900 °C with anatase crystallites of 47.6 nm still present (Table S1†). In the TiO_2/IL 10% sample (Fig. 2c), the anatase-to-rutile phase transition only started at 900 °C and again showed anatase crystallites (47.5 nm) beyond their thermodynamic limit of 35 nm. Raman spectroscopy measurements revealed that the temperature required to promote the solid-to-solid phase transition from anatase-to-rutile was dependent on the concentration of fluorine (Fig. S4†). For TiO_2 thermally treated at temperatures higher than 600 °C, the rutile phase was predominant over anatase; however, for TiO_2/IL 1% this predominance was only observed at 900 °C and for TiO_2/IL 10% anatase was the main phase even at 900 °C. UV-Vis measurements showed a significant redshift for the fluorinated samples, when compared with TiO_2, at the

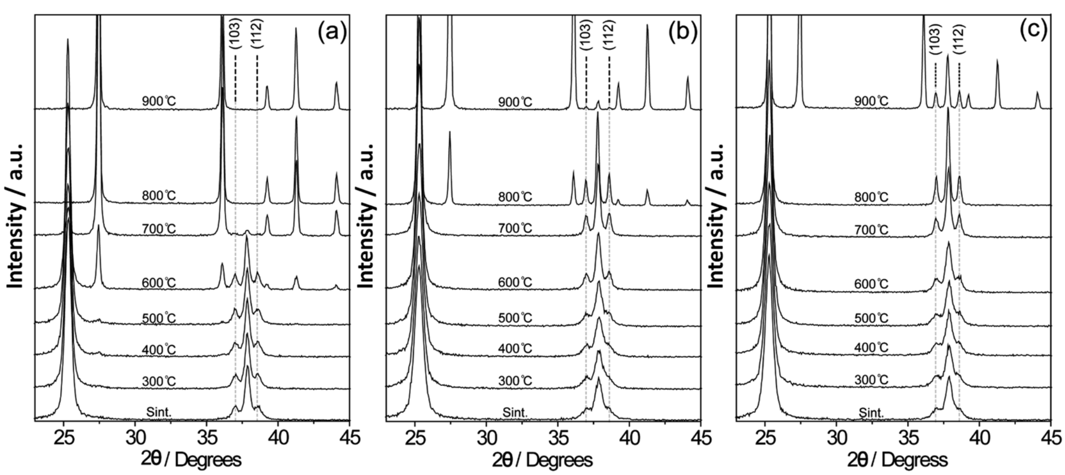

Fig. 2 (a–c) X-ray diffraction patterns of the as-synthesized and thermally treated samples from 300 °C to 900 °C for TiO_2, TiO_2/IL 1%, and TiO_2/IL 10%, respectively. Temperature dependence of the peaks related to the (103) and (112) planes.

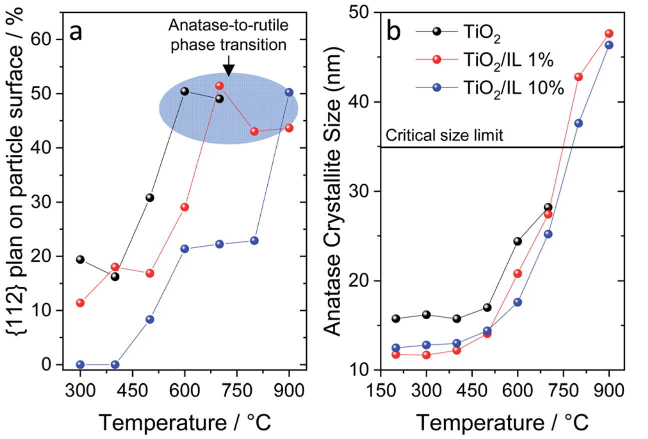

Fig. 3 (a) Percentage of {112} planes on the particle surface as a function of temperature highlighting the suppression of this facet by the IL compared to pure TiO_2. The data were extracted from the Wulff construction (see details in ESI Table S7†). (b) Anatase crystallite size for all samples, from the {101} planes (Table S3†), as a function of the temperature highlighting the crystallite critical size limit.

temperature at which the phase transition took place (Fig. S5†).[44–47]

As discussed earlier, the anatase-to-rutile phase transition temperature can be affected or controlled by how efficiently {112} twin boundaries interact with each other.[25,26] Therefore, we evaluated the effect of fluorine on the {112} facet growth by comparing the equivalent diffraction peaks related to the {112} plane at 38.60° and to the {103} plane at 36.95° (PDF number # 21-1272) (see Tables S2 and S3†).[48] For the fluorine–TiO_2 samples, the relative areas of the diffraction peaks ({112} and {103}) became nearly equivalent only at temperatures at which the material was about to undergo the anatase-to-rutile phase transition, while for pristine TiO_2 they remained similar to those for the synthesis at 600 °C. These results demonstrated that fluorine plays a critical role in suppressing the formation of {112} planes, thus delaying the anatase-to-rutile transition. The crystallite sizes for the {101}, {103}, {004} and {112} planes for TiO_2, TiO_2/IL 1% and TiO_2/IL 10% are presented in Tables S4–S6.† Although many reports in the literature have shown the use of fluoride to drive the preferential growth of {001} facets in TiO_2,[22,49,50] in the present work we have no clear evidence about the influence of the fluorinated ionic liquid on the {001} planes. In fact, neither hydrofluoric acid nor titanium tetrachloride was used in the synthesis and the F/Ti molar ratio in both samples was smaller than that commonly used to drive the preferential growth of {001} facets. We suggest that the amount of fluorine used to obtain TiO_2/IL 1% and TiO_2/IL 10% is enough to suppress the {112} planes, but not to affect the {001} growth.

Wulff grain construction was performed to confirm the effect of fluorine on the {112} plane at different temperatures (Fig. 3a and S6, and Tables S7–S10†).[51] Wulff principles are widely used in grain growth to determine which crystal geometrical shape has the minimum surface energy. The morphological equilibrium of the crystal corresponds to the minimization of the surface energy; from a thermodynamic perspective, the equilibrium crystal shape corresponds to the lowest free energy of the particle under specific conditions.[52,53] Fig. 3a shows the Wulff construction and highlights the {112} content, as a percentage, at which the anatase-to-rutile phase transition started. For pristine TiO_2, the contribution of the {112} facets increased from *ca.* 15% to 50% from 400 to 600 °C. TiO_2/IL 1% presented a similar trend, albeit from 500 to 700 °C instead. For TiO_2/IL 10%, three prominent features were observed: (i) the complete suppression of the {112} facets up to 400 °C; (ii) a contribution of only 20–25% of the {112} facets up to 800 °C; and (iii) a *ca.* 50% contribution at 900 °C, the temperature at which the anatase-to-rutile phase transition started for TiO_2/IL 10%. Additionally, Fig. 3b shows the crystallite sizes obtained from XRD measurements at different temperatures, highlighting the size limit within which anatase is thermodynamically stable. While a maximum size of *ca.* 28.2 nm was observed for TiO_2, the samples modified with fluorinated ionic liquid, TiO_2/IL 1% and TiO_2/IL 10%, exhibited crystallites of *ca.* 48 nm that surpass the thermodynamic limit. These results strongly suggested that achieving a specific fraction of the {112} facets might be the threshold limiting step for anatase-to-rutile phase transition and not the crystallite size itself.

FEG-SEM of TiO_2, TiO_2/IL 1% and TiO_2/IL 10% was performed to investigate the morphological changes before and after thermal treatment (Fig. 4). For pristine TiO_2, a sharp change in nanoparticle morphology was observed at 600 °C (blue box, Fig. 4), at which the sintering of relatively small TiO_2 nanoparticles led to the formation of much larger nanoparticles; this agreed with the anatase-to-rutile phase transition observed in XRD and Raman spectroscopy measurements. However, for TiO_2/IL 1% and TiO_2/IL 10% the sintering and formation of larger anatase nanoparticles were observed at 700 °C (green and red boxes, respectively, Fig. 4), which was a lower temperature than that observed for the anatase-to-rutile transition by XRD and Raman spectroscopy. In contrast to some previous reports, this demonstrated that the anatase-to-rutile phase transition limiting step is directly related to {112} facet concentration rather than a critical crystallite size of 35 nm.

EDX spectroscopy and XPS (Fig. S7–S10 and Table S3†) revealed the presence of fluorine in the samples prepared with ionic liquid prior to and after thermal treatment, while neither boron nor nitrogen were observed. HR-XPS of the F 1s region from the as-synthesized TiO_2/IL 1% and TiO_2/IL 10% showed a peak at 684.6 eV which was associated with adsorbed F^- ions on the TiO_2 surface (Fig. S10b and S10c†).[54] However, after thermal treatment at 500 °C, an additional peak at 687.8 eV was observed which was attributed to the incorporation of fluorine atoms into the TiO_2 structure (Figure S10e and S10f†). This suggested that the fluorine ions were coordinating to surface Ti^{4+} and Ti^{3+} ions, impacting the anatase-to-rutile phase transition.[55,56]

Photocurrent *versus* voltage (*I–V*) measurements of DSSCs assembled with TiO_2, TiO_2/IL 1%, and TiO_2/IL 10% were carried out (Fig. S11†) and the following parameters were measured from the assembled devices: the short-circuit current (I_{sc}), open-circuit voltage (V_{oc}), Fill Factor (FF) and efficiency (η) (Table 1). The power conversion efficiencies (under AM 1.5G illumination)

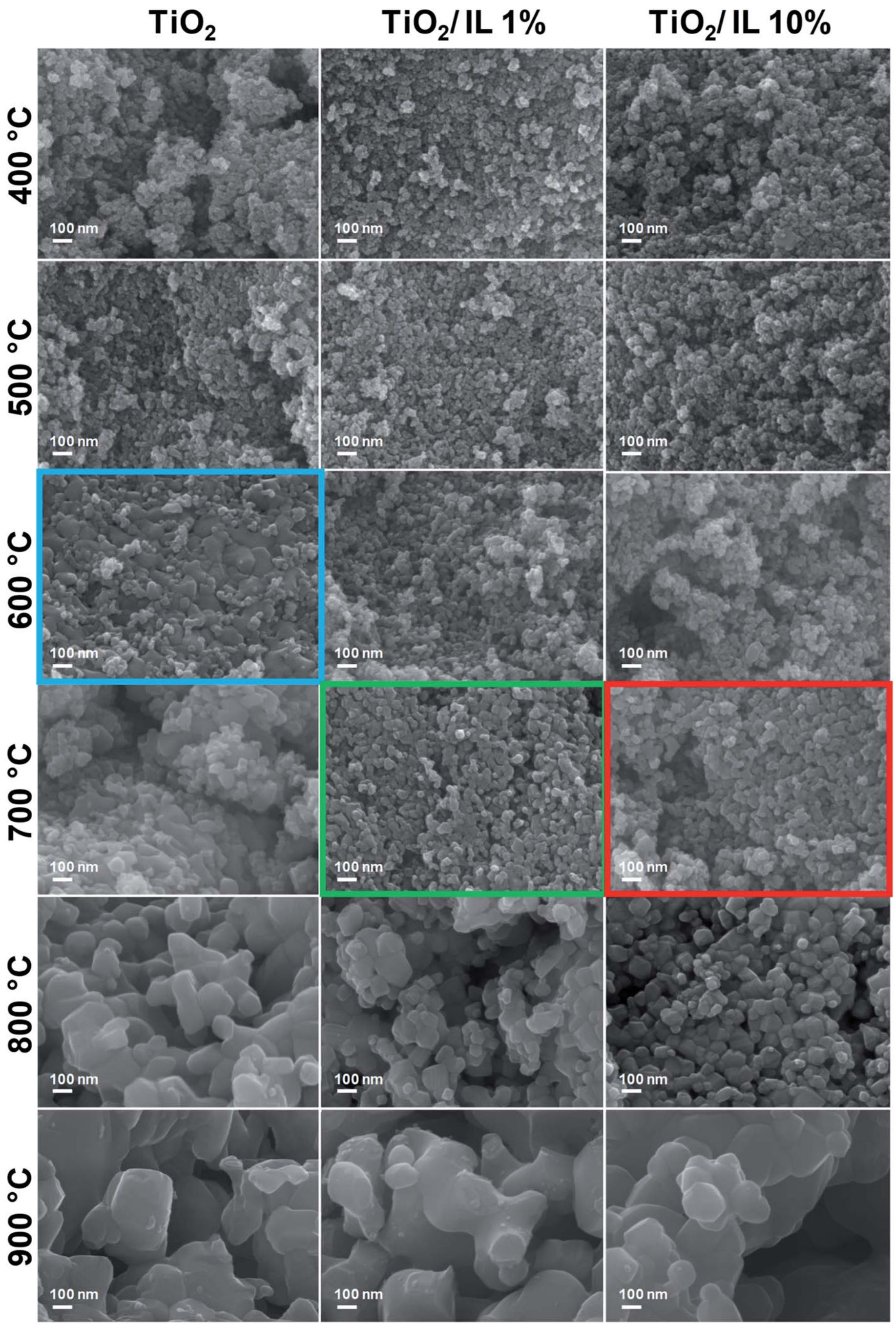

Fig. 4 FEG-SEM images of TiO_2, TiO_2/IL 1%, and TiO_2/IL 10% thermally treated from 300 °C to 900 °C. These images clearly show that TiO_2 morphological changes occur at different temperatures for the fluorinated TiO_2 nanoparticles (green and red boxes) when compared with pure TiO_2 (blue box).

Table 1 Electrical parameters, FF and efficiency obtained from the assembled DSSCs

Sample	I_{sc} (mA)	V_{oc} (V)	$I_{max}V_{max}$	FF	η
TiO_2	14.50	0.71	5.50	55%	5.50%
TiO_2/IL 1%	14.75	0.71	5.96	57%	5.96%
TiO_2/IL 10%	15.12	0.73	6.35	58%	6.35%

of standard TiO_2, TiO_2/IL 1%, and TiO_2/IL 10% were 5.50%, 5.96%, and 6.35%, respectively. The 15% enhancement in efficiency found for TiO_2/IL 10%, when compared to TiO_2, can be ascribed to the red-shift shown by the fluorinated samples. Additionally, it could be due to the suppression of rutile phase growth for the TiO_2 fluorinated samples during the sintering of the device assembly (Fig. S12†).[57] This may lead to a decrease in the density of defects in the fluorinated samples when compared to pristine TiO_2, which can act as recombination centers for photogenerated electron–hole pairs.[58–60]

Conclusions

An ionic liquid ($BMIm \cdot BF_4$) was used in the hydrothermal synthesis of TiO_2, resulting in fluorinated anatase phase nanoparticles greater in size than the previously determined 35 nm size limit. Fluorine favored the formation of the anatase phase at very low temperatures and contributed to the maintenance of this phase by hindering the growth of the {112} planes. This delayed the anatase-to-rutile phase transition, requiring much higher temperatures than usually observed for TiO_2. Wulff construction along with analyses by XPS, XRD, and Raman spectroscopy showed that the {112} facet played the main role in the anatase-to-rutile phase transition of TiO_2. These results strongly suggested that achieving a specific fraction of the {112} facets might be the threshold limiting step for anatase-to-rutile phase transition. Our findings demonstrate that the formation of {112} facets on the TiO_2 surface can be finely tuned by altering the concentration of fluorinated ionic liquid in the TiO_2 synthesis, enabling precise control of the anatase-to-rutile phase transition for a wide range of temperatures. DSSCs assembled with mesoporous layers based on TiO_2/IL 1% and TiO_2/IL 10% presented an improvement of the photocurrent and fill factor, and 15% greater efficiency when compared to pristine TiO_2.

Conflicts of interest

There are no conflicts to declare.

Acknowledgements

The authors are grateful for financial support from the following Brazilian agencies: Conselho Nacional de Desenvolvimento Científico e Tecnológico (grant 408182/2016-4), Fundação de Amparo à Pesquisa do Estado do Rio Grande do Sul and CAPES. JAF would like to acknowledge the University of Nottingham Beacons of Excellence: Propulsion Futures & Green Chemicals and EPSRC: LiPPS XPS system, and EP/K005138/1 "University of Nottingham Equipment Account" for providing financial support for this work and the Nanoscale and Microscale Research Centre (University of Nottingham, UK) for access to XPS facilities.

References

1 K. Jacobs, D. Zaziski, E. C. Scher, A. B. Herhold and A. P. Alivisatos, Activation Volumes for Solid-Solid Transformations in Nanocrystals, *Science*, 2001, **293**, 1803–1806.

2 D. Zhang, G. Li, X. Yang and J. C. Yu, A micrometer-size TiO_2 single-crystal photocatalyst with remarkable 80% level of reactive facets, *Chem. Commun.*, 2009, 4381–4383.

3 R. Shi and Y. Chen, Controlled Formation of Defective Shell on TiO_2 (001) Facets for Enhanced Photocatalytic CO_2 Reduction, *ChemCatChem*, 2019, **11**, 2270–2276.

4 G. Liu, H. G. Yang, J. Pan, Y. Q. Yang, G. Q. Lu and H. Cheng, Titanium dioxide crystals with tailored facets, *Chem. Rev.*, 2014, **114**(19), 9559–9612.

5 K. Qi, D. Li, J. Fu, L. Zhu, X. Duan, Q. Qin, G. Wang and W. Zheng, Elucidating ionic liquid environments that affect the morphology of TiO_2 nanocrystals: a DFT+D study, *J. Phys. Chem. C*, 2014, **118**, 23320–23327.

6 J. Joo, B. Y. Chow, M. Prakash, E. S. Boyden and J. M. Jacobson, Face-selective electrostatic control of hydrothermal zinc oxide nanowire synthesis, *Nat. Mater.*, 2011, **10**, 596–601.

7 A. S. Barnard and L. A. Curtiss, Prediction of TiO_2 Nanoparticle Phase and Shape Transitions Controlled by Surface Chemistry, *Nano Lett.*, 2005, **5**, 1261–1266.

8 M. Batzill, E. H. Morales and U. Diebold, Influence of Nitrogen Doping on the Defect Formation and Surface Properties of TiO_2 Rutile and Anatase, *Phys. Rev. Lett.*, 2006, **96**, 26103.

9 H. Zhang and J. F. Banfield, Understanding Polymorphic Phase Transformation Behavior during Growth of Nanocrystalline Aggregates: Insights from TiO_2, *J. Phys. Chem. B*, 2000, **104**, 3481–3487.

10 M. Pal, J. G. Serrano, P. Santiago and U. Pal, Size-Controlled Synthesis of Spherical TiO_2 Nanoparticles: Morphology, Crystallization, and Phase Transition, *J. Phys. Chem. C*, 2007, **111**, 96–102.

11 H. Zhang and J. F. Banfield, Size Dependence of the Kinetic Rate Constant for Phase Transformation in TiO_2 Nanoparticles, *Chem. Mater.*, 2005, **17**, 3421–3425.

12 D. Li, H. Wang, D. Xiao, M. Song, B. Legg and J. Chun, Investigating the magnitude and source of orientation-dependent interactions between TiO_2 crystal surfaces, *Nanoscale*, 2017, **9**, 10173–10177.

13 D. Majumder and S. Roy, Non-fluorinated synthesis of anatase TiO_2 with dominant {001} facets: influence of faceted structures on formaldehyde sensitivity, *New J. Chem.*, 2017, **41**, 7591–7597.

14 J. Pan, G. Liu, G. Q. Lu and H. M. Cheng, On the True Photoreactivity Order of {001}, {010}, and {101} Facets of Anatase TiO_2 Crystals, *Angew. Chem.*, 2011, **50**, 2133–2137.

15 M. Bellardita, C. Garlisi, A. M. Venezia, G. Palmisano and L. Palmisano, Influence of fluorine on the synthesis of anatase TiO_2 for photocatalytic partial oxidation: are exposed facets the main actors?, *Catal. Sci. Technol.*, 2018, **8**, 1606–1620.

16 X. Han, Q. Kuang, M. Jin, Z. Xie and L. Zheng, Synthesis of Titania Nanosheets with a High Percentage of Exposed (001) Facets and Related Photocatalytic Properties, *J. Am. Chem. Soc.*, 2009, **131**, 3152–3153.

17 D. Zhang, G. Li, X. Yang and C. J. Yu, A micrometer-size TiO_2 single-crystal photocatalyst with remarkable 80% level of reactive facets, *Chem. Commun.*, 2009, **29**, 4381–4383.

18 X. Han, X. Wang, S. Xie, Q. Kuang, J. Ouyang, Z. Xie and L. Zheng, Carbonate ions-assisted syntheses of anatase

TiO_2 nanoparticles exposed with high energy (001) facets, *RSC Adv.*, 2012, **2**, 3251–3253.

19 F. Lin, Y. Chen, L. Zhang, D. Mei, L. Kovarik, B. Sudduth, H. Wang, G. Gao and Y. Wang, Single-Facet Dominant Anatase TiO_2 (101) and (001) Model Catalysts to Elucidate the Active Sites for Alkanol Dehydration, *ACS Catal.*, 2020, **10**, 4268–4279.

20 Y. Wu, F. Gao, H. Wang, L. Kovarik, B. Sudduth and Y. Wang, Probing Acid–Base Properties of Anatase TiO_2 Nanoparticles with Dominant {001} and {101} Facets Using Methanol Chemisorption and Surface Reactions, *J. Phys. Chem. C*, 2021, **125**(7), 3988–4000.

21 Z. Tan, K. Sato, S. Takami, C. Numako, M. Umetsu, K. Soga, M. Nakayama, R. Sasaki, T. Tanaka, C. Ogino, A. Kondo, K. Yamamoto, T. Hashishin and S. Ohara, Particle size for photocatalytic activity of anatase TiO_2 nanosheets with highly exposed {001} facets, *RSC Adv.*, 2013, **3**, 19268–19271.

22 H. G. Yang, C. H. Sun, S. Z. Qiao, J. Zou, G. Liu, S. C. Smith, H. M. Cheng and G. Q. Lu, Anatase TiO_2 single crystals with a large percentage of reactive facets, *Nature*, 2008, **453**, 638–641.

23 T. Butburee, P. Kotchasarn, P. Hirunsit, Z. Sun, Q. Tang, P. Khemthong, W. Sangkhun, W. Thongsuwan, P. Kumnorkaew, H. Wang and K. Faungnawakij, New understanding of crystal control and facet selectivity of titanium dioxide ruling photocatalytic performance, *J. Mater. Chem. A*, 2019, **7**, 8156.

24 P. Voepel, C. Seitz, J. M. Waack, S. Zahn, T. Leichtwei, A. Zaichenko, D. Mollenhauer, H. Amenitsch, M. Voggenreiter, S. Polarz and B. M. Smarsly, Peering into the Mechanism of Low-Temperature Synthesis of Bronze-type TiO_2 in Ionic Liquids, *Cryst. Growth Des.*, 2017, **17**, 5586–5601.

25 R. L. Penn and J. F. Banfield, Formation of rutile nuclei at anatase {112} twin interfaces and the phase transformation mechanism in nanocrystalline titania, *Am. Miner.*, 1999, **84**, 871–876.

26 S.-C. Zhu, S.-H. Xie and Z.-P. Liu, Nature of Rutile Nuclei in Anatase-to-Rutile Phase Transition, *J. Am. Chem. Soc.*, 2015, **137**, 11532–11539.

27 N. Satoh, T. Nakashima and K. Yamamoto, Metastability of anatase: size dependent and irreversible anatase-rutile phase transition in atomic-level precise titania, *Sci. Rep.*, 2013, **3**, 1959.

28 H. Wu, Y. Yang, Y. Ou, B. Lu, J. Li, W. Yuan, Y. Wang and Z. Zhang, Early Stage Growth of Rutile Titania Mesocrystals, *Cryst. Growth Des.*, 2018, **18**(8), 4209–4214.

29 R. D. Shannon and J. A. Pask, Kinetics of the Anatase-Rutile Transformation, *J. Am. Ceram. Soc.*, 1965, **48**, 391–398.

30 A. A. Gribb and J. F. Banfield, Particle size effects on transformation kinetics and phase stability in nanocrystalline TiO_2, *Am. Mineral.*, 1997, **82**, 717–728.

31 X. Mettan, J. Jaćimović, O. S. Barišić, A. Pisoni, I. Batistić, E. Horváth, S. Brown, L. Rossi, P. Szirmai, B. Farkas, H. Berger and L. Forró, Tailoring thermal conduction in anatase TiO_2, *Commun. Phys.*, 2019, **2**, 123.

32 X. Bai, T. Li, U. Gulzar, E. Venezia, L. Chen, S. Monaco, Z. Dang, M. Prato, S. Marras, P. Salimi, S. Fugattini, C. Capiglia and R. P. Zaccaria, Towards enhanced sodium storage of anatase TiO_2 *via* a dual-modification approach of Mo doping combined with AlF_3 coating, *Nanoscale*, 2020, **12**, 15896–15904.

33 P. Mazzolini, P. Gondoni, V. Russo, D. Chrastina, C. S. Casari and A. Li Bassi, Tuning of Electrical and Optical Properties of Highly Conducting and Transparent Ta-Doped TiO_2 Polycrystalline Films, *J. Phys. Chem. C*, 2015, **119**(13), 6988–6997.

34 E. Ringe, R. P. Van Duyne and L. D. Marks, Wulff Construction for Alloy Nanoparticles, *Nano Lett.*, 2011, **11**(8), 3399–3403.

35 C. Boukouvala and E. Ringe, Wulff-Based Approach to Modeling the Plasmonic Response of Single Crystal, Twinned, and Core–Shell Nanoparticles, *J. Phys. Chem. C*, 2019, **123**(41), 25501–25508.

36 S. Yang, B. X. Yang, L. Wu, Y. H. Li, P. Liu, H. Zhao, Y. Y. Yu, X. Q. Gong and H. G. Yang, *Nat. Commun.*, 2014, **5**, 5355.

37 S. Ito, T. Murakami, P. Comte, P. Liska, C. Gratzel, M. Nazeeruddin and M. Gratzel, Fabrication of thin film dye sensitized solar cells with solar to electric power conversion efficiency over 10%, *Thin Solid Films*, 2008, **516**, 4613–4619.

38 K. Momma and F. Izumi, VESTA 3 for three-dimensional visualization of crystal, volumetric and morphology data, *J. Appl. Cryst.*, 2011, **44**, 1272–1276.

39 N. Rahimi, R. A. Pax and E. MacA Gray, Review of functional titanium oxides. I: TiO_2 and its modifications, *Prog. Solid State Chem.*, 2016, **44**, 86–105.

40 E. Binetti, A. Panniello, R. Tommasi, A. Agostiano, S. Fantini, M. L. Curri and M. Striccoli, Interaction of TiO_2 Nanocrystals with Imidazolium-Based Ionic Liquids, *J. Phys. Chem. C*, 2013, **117**, 12923–12929.

41 T. Alammar, H. Noei, Y. Wang and A. V. Mudring, Mild yet phase-selective preparation of TiO_2 nanoparticles from ionic liquids – a critical study, *Nanoscale*, 2013, **5**, 8045–8055.

42 X. Duan, J. Ma, J. Lian and W. Zheng, The art of using ionic liquids in the synthesis of inorganic nanomaterials, *CrystEngComm*, 2014, **16**(13), 2550–2559.

43 P. Voepel and B. M. Smarsly, Synthesis of Titanium Oxide Nanostructures in Ionic Liquids, *Z. Anorg. Allg. Chem.*, 2017, **643**(1), 3–13.

44 S. Winardi, R. R. Mukti, K. P. Kumar, J. Wang, W. Wunderlich and T. Okubo, Critical Nuclei Size, Initial Particle Size and Packing Effect on the Phase Stability of Sol-Peptization-Gel-Derived Nanostructured Titania, *Langmuir*, 2010, **26**(7), 4567–4571.

45 M. Fernández-García, X. Wang, C. Belver, J. C. Hanson and J. A. Rodriguez, Anatase-TiO_2 Nanomaterials: Morphological/Size Dependence of the Crystallization and Phase Behavior Phenomena, *J. Phys. Chem. C*, 2007, **111**, 674–682.

46 D. Casotti, M. Ardit, R. Dinnebier, M. Dondi, F. Matteucci, I. Zama and G. Cruciani, Limited Crystallite Growth upon

Isothermal Annealing of Nanocrystalline Anatase, *Cryst. Growth Des.*, 2015, **15**(5), 2282–2290.
47 Y. Wang, B. Wen, A. Dahal, G. A. Kimmel, R. Rousseau, A. Selloni, N. G. Petrik and Z. Dohnálek, Binding of Formic Acid on Anatase TiO_2(101), *J. Phys. Chem. C*, 2020, **124**(37), 20228–20239.
48 F. Scarpelli, T. F. Mastropietro, T. Poerio and N. Godbert, Mesoporous TiO_2 Thin Films: State of the Art, *Titan. Dioxide Mater. A Sustain. Environ.*, 2018, 57–80.
49 F. Pellegrino, E. Morra, L. Mino, G. Martra, M. Chiesa and V. Maurino, Surface and Bulk Distribution of Fluorides and Ti^{3+} Species in TiO_2 Nanosheets: Implications on Charge Carrier Dynamics and Photocatalysis, *J. Phys. Chem. C*, 2020, **124**(5), 3141–3149.
50 W. Yang, W. Xu, Y. Wang, D. Chen, X. Wang, Y. Cao, Q. Wu, J. Tu and C. Zhen, Photoelectrochemical Glucose Biosensor Based on the Heterogeneous Facets of Nanocrystalline TiO_2/Au/Glucose Oxidase Films, *ACS Applied Nano Materials*, 2020, **3**(3), 2723–2732.
51 D. González, B. Camino, J. Heras-Domingo, A. Rimola, L. Rodríguez-Santiago, X. Solans-Monfort and M. Sodupe, BCN-M: A Free Computational Tool for Generating Wulff-like Nanoparticle Models with Controlled Stoichiometry, *J. Phys. Chem. C*, 2020, **124**(1), 1227–1237.
52 P. L. Hansen, J. B. Wagner, S. Helveg, J. R. Rostrup-Nielsen, B. S. Clausen and H. Topsøe, Atom-Resolved Imaging of Dynamic Shape Changes in Supported Copper Nanocrystals, *Science*, 2002, **295**, 2053–2055.
53 F. Lai, Y. Chen and H. Guo, Surface energies of non-centrosymmetric nanocrystals by the inverse Wulff construction method, *Phys. Chem. Chem. Phys.*, 2019, **21**, 16486–16496.
54 M. V. Dozzi and E. Selli, Doping TiO_2 with p-block elements: Effects on photocatalytic activity, *J. Photochem. Photobiol. C: Photochem. Rev.*, 2013, **14**, 13–28.
55 J. C. Yu, J. Yu, W. Ho, Z. Jiang and L. Zhang, Effects of F^- Doping on the Photocatalytic Activity and Microstructures of Nanocrystalline TiO_2 Powders, *Chem. Mater.*, 2002, **14**, 3808–3816.
56 E. M. Samsudin, S. B. A. Hamid, J. C. Juan, W. J. Basirun and G. Centi, Synergetic effects in novel hydrogenated F-doped TiO_2 photocatalysts, *Appl. Surf. Sci.*, 2016, **370**, 380–393.
57 V. Mansfeldova, M. Zlamalova, H. Tarabkova, P. Janda, M. Vorokhta, L. Piliai and L. Kavan, Work Function of TiO_2 (Anatase, Rutile, and Brookite) Single Crystals: Effects of the Environment, *J. Phys. Chem. C*, 2021, **125**(3), 1902–1912.
58 A. M. Czoska, S. Livraghi, M. Chiesa, E. Giamello, S. Agnoli, G. Granozzi, E. Finazzi, C. Di Valentin and G. Pacchioni, The Nature of Defects in Fluorine-Doped TiO_2, *J. Phys. Chem. C*, 2008, **112**, 8951–8956.
59 J. Yu, Y. Yang, R. Fan, L. Li and X. Li, Rapid Electron Injection in Nitrogen- and Fluorine-Doped Flower-Like Anatase TiO_2 with {001} Dominated Facets and Dye-Sensitized Solar Cells with a 52% Increase in Photocurrent, *J. Phys. Chem. C*, 2014, **118**(17), 8795–8802.
60 T. Su, Y. Yang, Y. Na, R. Fan, L. Li, L. Wei, B. Yang and W. Cao, An Insight Into the Role of Oxygen Vacancy in Hydrogenated TiO_2 Nanocrystals in the Performance of Dye Sensitized Solar Cells, *ACS Appl. Mater. Interfaces*, 2015, **7**, 3754–3761.